Aerosol and Air Quality Research

ORIGINAL RESEARCH
https://doi.org/10.4209/aaqr.230127

# Seasonal Particle Size Distribution and its Influencing Factors in a Typical Polluted City in North China

**Wenxin Wang[1], Xiaohua Wang[2], Xue Li[1], Chao Chen[1], Yu Wang[1], Zhiwen Xing[1], Kun Li[1], Min Wei[1,3], Xiao Sui[1,3*], Houfeng Liu[1,3*]**

[1] College of Geography and Environment, Shandong Normal University, Jinan 250014, China
[2] Rizhao Polytechnic, Rizhao 276826, China
[3] Center for Environmental Technology and Policy Research, Shandong Normal University, Ji'nan 250014, China

## ABSTRACT

In this study, the particle size distribution and its influencing factors were conducted using a multi-channel particle size sensor coupled with Pearson and generalized additive model (GAM) during winter 2021 to autumn 2022 in Jinan, North China. The results revealed that heavy pollution episodes were mainly caused by fine particles ($PM_{<1}$ and $PM_{1\text{-}2.5}$) in winter and coarse particles ($PM_{2.5\text{-}10}$ and $PM_{>10}$) in spring. Pearson and generalized additive model (GAM) analysis indicated $PM_{2.5}$ was positively correlated with relative humidity (RH), CO, $NO_2$, $SO_2$, and $PM_{2.5\text{-}10}$ concentrations, negatively correlated with wind speed, $O_3$ and coarse particles ($PM_{>10}$) concentrations. Moreover, there was also a strong correlation between $PM_{2.5}$ concentration and meteorological-air pollutant factors interactions. $PM_{2.5\text{-}10}$ was found to be positively correlated with gaseous pollutants such as $NO_2$, $SO_2$, and CO, as well as RH and air pressure. Besides, $PM_{>10}$ was positively associated with CO, $SO_2$, and RH, but negatively correlated with $NO_2$ and wind speed. The particle size distribution was also effected by regional transport, particular in winter and spring. In detail, $PM_{2.5}$ and $PM_{2.5\text{-}10}$ were mainly transported from the east and north, $PM_{>10}$ mainly from the north and southwest in winter. In spring, particle matters were mainly transported from the northeast and southeast, and $PM_{2.5}$ was more influenced by northeast short-range transport. Local particulate generation was mainly raised by mobile sources from vehicles and industries such as oil refineries, chemical plant and steel plants. Therefore, the emission controls on VOCs, $NO_2$, $SO_2$ and regional joint pollution prevention are preferred to reduce urban air pollution in future.

**Keywords:** Air pollution, Size distribution, Generalized additive model, Long-range transport

OPEN ACCESS

**Received:** June 1, 2023
**Revised:** October 21, 2023
**Accepted:** November 30, 2023

*** Corresponding Authors:**
Xiao Sui
suixiao@sdnu.edu.cn
Houfeng Liu
110027@sdnu.edu.cn

**Publisher:**
Taiwan Association for Aerosol Research
**ISSN:** 1680-8584 print
**ISSN:** 2071-1409 online



## 1 INTRODUCTION

In recent years, air pollution characterized by particle matter has become one of the most concerned environmental pollution issues in the past decade (Zhang *et al.*, 2015b; Han *et al.*, 2016; Qiao *et al.*, 2022). More than two million deaths are estimated to occur globally each year as a direct consequence of air pollution through damage to the lungs and the respiratory system (Shah *et al.*, 2013). Of these deaths, about 0.21 million were caused by particle matter (Chuang *et al.*, 2011; Shah *et al.*, 2013). The study of particle size distribution characteristics can provide effective information for the sources, behaviour and mechanism of formation of particles in the atmosphere (Parmar *et al.*, 2001). Pollutants from different sources are more likely to be enriched in particle matter of certain specific particle sizes (Allen *et al.*, 2001). Particularly, haze pollution is greatly influenced by the particle concentration, size distribution, chemical composition and mixing state (Tan *et al.*, 2016; Xiang *et al.*, 2017).

Related studies carried out in China found there were large differences in particle size between the north and the south, with the peaks of particle size distribution in Chengdu, Tianjin and Hangzhou mainly concentrated in the 1.1–2.1 µm, 0.7–1.1 µm and 9.0–10.0 µm; 0.8–1.1 µm and 9.0–10.0 µm; 0.7–1.1 µm and 9.0–10.0 µm, respectively (Wang *et al.*, 2017). As a province with dense industry and population, Shandong was one of the major particulate emissions sources, and the distribution of particle matter exhibited spatial clustering and differential patterns (Zhang *et al.*, 2007). The correlation with meteorological factors varied with the seasons, with dust having a significant impact on particle matter concentrations (Yu *et al.*, 2021). In Jinan, capital of Shandong province, the particle matter was concentrated within the range of 0.1–2.5 µm, and the concentration and particle size distribution of particle matter exhibited distinct seasonal variations. The formation of particle matter was mainly attributed to traffic emissions and the transportation of particles from the suburbs (Xu *et al.*, 2011; Wang *et al.*, 2014). The particle size distribution in Beijing appeared a triple-peaked distribution in urban areas and a double-peaked distribution in suburban areas, with peaks mainly in the 0.43–0.65 µm and 9.0–10.0 µm particle size segments (Tan *et al.*, 2016). In Hong Kong, the size distribution was concentrated at 0.4–0.7 µm and 8.0–9.5 µm (Gao *et al.*, 2016). On a global scale, previous studies showed that the peak particle size distribution in Turin mainly around 1 µm and 5 µm, which was influenced by the combination of coal combustion, motor vehicle emissions, construction dust and other pollution sources (Malandrino *et al.*, 2016). In Egypt, the particle size was mainly in the 0.46–0.75 µm and 8.5–10.0 µm, and the specific distribution pattern varies greatly with the pollution degree (Moustafa *et al.*, 2015). Athens particle size distribution varies greatly with the seasons, the percentage ranking was found as follows: $PM_{0.95} > PM_{3.0\text{-}7.2} > PM_{7.2\text{-}10.0} > PM_{1.5\text{-}3.0}$, most particle number peaks in autumn are fine particles while in winter are coarse particles. This is due to the fine particle could be emitted from straw burning in autumn, and the inverse temperature weather in winter is more conducive to the formation of coarse particle matter (Karanasiou *et al.*, 2007).

In recent years, machine learning techniques such as random forest have been widely applied to investigate the non-relationship between $PM_{2.5}$ and meteorological factors (Ly *et al.*, 2021). Numerous scientific studies have found that the synergies between different pollutants, meteorological conditions and topographic features may influence the sources and dispersion of particle matter (Deng *et al.*, 2012; Chen *et al.*, 2014; Fu *et al.*, 2014; Liu *et al.*, 2017; Wang *et al.*, 2019). Various methods including particle growth rate (GR) calculations using both Log Normal and Max Concentration, aerosol optical depth (AOD) model simulations of near-surface emission sources, etc. have been used to explore the trends and influencing factors of air pollutants (Liu *et al.*, 2009; Li *et al.*, 2017a). However, research utilizing statistical methods to investigate particle size distribution and its influencing factors has not been widely reported in the study area during recent years. Generalized additive model (GAM) can fit the response and explanatory variables by the smooth spline functions, kernel function, and regression smooth function. It prefers to minimize residuals and maximize minimalism (Wu and Zhang, 2019). Compared with other statistical models, GAM are more flexible and freer thus it is suited to our study to analyze complex nonlinear relationships (Westervelt *et al.*, 2016; Zhai *et al.*, 2019). Thus, GAM can reflect the degree of correlation between different particle sizes and effect factors intuitively. Furthermore, it can provide a general framework for air pollution, which could help researchers and policy makers and to understand regional ambient air quality changes (Li *et al.*, 2017b). Consequently, research comparing the particle size distribution characteristics and influencing factors is essential for pollution prevention as well as on the sources and formation of particle matter.

As one of the polluted capital cities in north China, Jinan has been suffering from severe particle pollution in recent years (Wang *et al.*, 2016; Tian *et al.*, 2020; Yu *et al.*, 2021). In this study, particle size from 0.25–35.0 µm along with six conventional air pollutants ($PM_{2.5}$, $PM_{10}$, $SO_2$, CO, $NO_2$, and $O_3$) and meteorological elements from two stations (municipal super station and municipal monitoring station) were used to explore the factors of particle size distribution in the heavy pollution process from winter 2021 to autumn 2022. Mantel test, Pearson analysis and GAM were carried out to further confirm the influence from precursors and meteorological conditions. Moreover, the effects of long-range transport on particle matter pollution and particle size characteristics were discussed together with GAM results. This study aimed to further understand the formation mechanisms of different particle sizes and then help relevant administrations to take targeted management measures under different meteorological conditions.

https://doi.org/10.4209/aaqr.230127

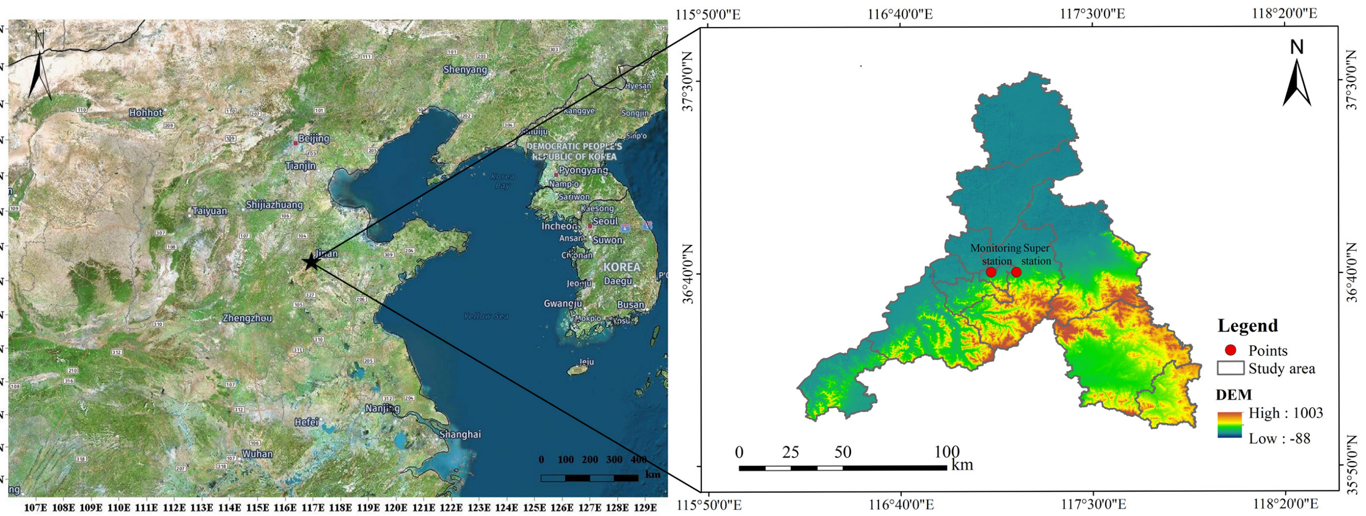


**Fig. 1.** (a) The position of Jinan, 36°40′N, 117°00′E. (b) The position of the Monitoring station, 36°67′N, 117°17′E, and Super station, 36°67′N, 117°06′E.

## 2 METHODS

### 2.1 Research Area

Jinan is located in the southeast of the North China Plain, bordering the Beijing-Tianjin-Hebei economic circle in the north and the Yangtze River Delta economic circle in the south, with a total area of 10,244.45 km$^2$. By November 2021, there were 9,202,400 permanent residents. Geographical location ranges from 36°01′N to 37°32′N and 116°11′E to 117°44′E. The terrain is high in the south and low in the north, surrounded by mountains on three sides. The geographical location of Jinan, the positions of the monitoring station and the super station in Jinan, are depicted in Fig. 1. Compared to other monitoring stations, the Atmospheric Environment Super Monitoring Station of the Shandong Provincial Department of Ecology and Environment (referred to as the "Super station") has a more comprehensive array of instruments and a larger scale. Currently, it is equipped with a total of 21 devices, including Thermo Scientific Model-42i, Thermo Scientific Model-48i, Thermo Scientific Model-5030, and MetOne BAM-1020, and so on.

### 2.2 Data

The data of $PM_{10}$, $PM_{2.5}$, $SO_2$, CO, $NO_2$, $O_3$ and meteorological factors from November 1, 2021 to October 31, 2022 were obtained from the Integrated Atmospheric Observation Platform of Shandong Province (http://123.232.114.72:8096/shandong/login). During the sample time, November 1, 2021 to January 31, 2022 were defined as winter, February 1, 2022 to April 30, 2022 were defined as spring, May 1, 2022 to July 31, 2022 were defined as summer, and August 1, 2022 to October 31, 2022 were defined as autumn. The average concentration of pollutants in Jinan was calculated with reference to GB3095-2012. The long-range transmission data were acquired from ftp://arlftp.arlhq.noaa.gov/pub/archives/reanalysis. The particle size spectrum data are measured by SDS029, which is a multi-channel particle size sensor comprising 31 particle size channels ranging from 0.3 to 35.0 µm (including $PM_{0.3}$, $PM_{1.0}$, $PM_{2.5}$, $PM_{4.0}$, $PM_{10.0}$, TSP, etc.). Based on the principle of single-particle laser scattering and following a calibration process, particle numbers and mass concentrations for each channel are output (More information on the data and sampling methods can be found in the Supporting Methods of Supplementary Information).

### 2.3 Generalized Additive Model (GAM)

Generalized additive model (GAM) is a flexible regression model based on prediction (Eq. (1)) (Verbeke, 2007). This model can perform more reasonable nonlinear fitting analysis than the traditional generalized linear models (Zhang *et al.*, 2015a). In contrast to the generalized linear model, the independent and dependent variables of the generalized addable model can be of arbitrary form, which is done to find a more suitable fitting curve (Sorek-Hamer *et al.*, 2013; Ma *et al.*, 2020). Meanwhile, GAM requires less data and can be applied to a variety of distribution types (e.g., Poisson distribution). The basic equation of GAM is as follows (Eq. (1)):

$$g[E(Y)] = \beta_0 + f_1(X_1) + f_2(X_2) + \ldots + f_n(X_n) + \varepsilon \tag{1}$$

where $Y$ is the response variable; $E(Y)$ is the mathematical expectation of response variable; $g$ represents the connection function; $\beta_0$ is the intercept; $\varepsilon$ is the truncation error; $X_1$, …, $X_n$ represents the explanatory variables; $f_1$, …, $f_n$ represents the smoothing function connecting explanatory variables, which is usually fitted using a smooth spline function. The results of the analysis were characterized by parameters such as degrees of freedom, $P$-value, $F$-value, adjusted coefficient of determination ($R^2$), and variance interpretation rate. When the degree of freedom is greater than 1, it means that the relationship between the influencing factor and the response variable is nonlinear, and the larger the value of the degree of freedom, the more significant the nonlinear relationship; when the degree of freedom is equal to 1, it means that the relationship between the influencing factor and the response variable is linear. In addition, the selection process of the optimal model is done with the help of the Akaike information criterion (AIC) (Norman, 2000; Lin *et al.*, 2018; Ma *et al.*, 2020). The smaller the AIC, the better the model fit (Table S2).

In this study, the hourly mass concentration of $PM_{2.5}$ was used as the response variable, and the hourly values of pertinent environmental factors were utilized as the explanatory variables. Firstly, a Pearson analysis on $PM_{2.5}$ and all the explanatory variables were conducted (Fig. 4). Secondly, correlation coefficients were applied to discern the degree of correlation between the factors. Significantly positive correlations between $PM_{2.5}$ and temperature (T), relative humidity (RH), CO, $NO_2$, $SO_2$, and $PM_{2.5\text{-}10}$ were detected by data preprocessing. However, no variable had a correlation coefficient greater than 8 with $PM_{2.5}$, so explanatory variables were not combined and censored.

The variance inflation factor (VIF) was applied to quantify the degree of multicollinearity. The stronger the multicollinearity, the larger the VIF value. If a predictor variable is not correlated with other predictor variables, the VIF of that predictor variable is 1 (He and Lin, 2017). The threshold was set to 5 and the VIF of each explanatory variable was less than 5 in this study (Table 2) and there is no multicollinearity (Huang *et al.*, 2020). The hourly concentration of $PM_{2.5}$ in the model conforms to the Poisson distribution and is constructed on its basis, so the log link function is used to connect the response variable to the explanatory variables (Thurston *et al.*, 2000). The "car" package to computed VIF functions and the "mgcv" package were used to computed GAMs in R 4.2.0 and Rstudio 12.0 (https://posit.co/download/rstudio-desktop/).

$$\log(PM_{2.5}) = \beta_0 + s(time) + DOW + s(T) + s(RH) + s(P) + s(WS) + s(CO) + s(NO_2) + s(SO_2) + s(O_3) + s(PM_{2.5\text{-}10}) + s(PM_{>10}) + \varepsilon \tag{2}$$

where *time* is a number ranging from 1 to 3746 (Calculated from heavy pollution days), that is used in the calculation to assess long-term trends and seasonality; *DOW* (day of the week, ranging from 1 to 7) is a dummy variable that is used to control the weekend effect; $\beta_0$ is the intercept; $\varepsilon$ is the truncation error. $T$ is the temperature (°C), $RH$ is the relative humidity, $P$ is the air pressure, and $WS$ is the wind speed (Eq. (2)).

In the multi-factor GAM, there are forty-five interactive influencing factors (Eq. (3)):

$$\log(PM_{2.5}) = \beta_0 + s(time) + DOW + \sum_{i=1}^{n} s(P_i, M_i) + \varepsilon \tag{3}$$

where $P_i$ and $M_i$ represents the environmental explanatory variables that affect the $PM_{2.5}$ concentration, and $s(P_i, M_i)$ represents the interaction term between factor $P$ and factor $M$. The remaining explanatory variables are the same as in Eq. (2).

## 2.4 Long-range Transport Model

The hybrid single-particle Lagrangian integrated trajectory (HYSPLIT) model was applied to simulate the 24 h backward trajectory of the Jinan observation site (36°67′N, 112°32′E) in winter 2021 and autumn 2022, 90.0 m a.s.l and time interval was set to 1 h.

Concentration weighted trajectory (CWT) was applied to calculate the pollution concentration values for each trajectory in the grid, which were then weighted according to the residence time. The function to calculate the CWT value is expressed as (Eq. (4)) (Li *et al.*, 2020a):

$$C_{ij} = \frac{\sum_{i=1}^{M} C_l \tau_{ijl}}{\sum_{i=1}^{M} \tau_{ijl}} \tag{4}$$

where the denominator represents the concentration sum in the grid; $\tau_{ijl}$ represents the time node; $C_l$ represents the trajectory node.

# 3 RESULTS AND DISCUSSION

## 3.1 Overview of Particulate Pollution

### 3.1.1 Time distribution of particle size

The particle size distribution of Jinan from winter 2021 to autumn 2022 were mainly from 1.0–13.0 µm. In general, the particle pollution in winter were more serious than other seasons. (Fig. 2(a)). During the observation period, the most polluted period was winter 2021 with the particle size distribution was mainly 0.5–10.0 µm. There were 7 heavy pollution processes with particle size distribution of 1.0–10.0 µm, 1.3–10.0 µm, 0.3–6.8 µm, 0.3–10.0 µm, 1.3–10.0 µm and 0.35–4.1 µm respectively (as shown in Fig. 2). The secondary polluted season was spring 2022, and the particle size was concentrated around 0.8–18.0 µm. Three heavy pollution processes were detected during this episode with the main particle size distribution of 1.6–35.0 µm, 1.8–13.0 µm and 0.35–13.0 µm respectively. This shows that the particle size in winter was smaller than in spring in general (detail analysis was shown in Section 3.1.2). Particulate pollution in summer and autumn 2022 were lighter than in winter 2021 and spring 2022, with the major particle size distribution of 1.0–10.0 µm.

During the observation period, the particle matter causing pollution was $PM_{2.5}$ and $PM_{2.5\text{-}10}$. Fine particle matter was small in size and light in mass, so they can easily suspended in the air. Particle pollution peaked during 7:00–12:00 and 17:00–1:00 with a 2.5–10.0 µm diameter. This phenomenon may be related to morning and evening peak vehicle emissions, vehicle brake wear, human production and domestic emissions (Fig. 2(b)) (Wei *et al.*, 2022). Low temperature, high relative humidity and low wind speed appeared during early morning and night also favored the accumulation of particle matter (Bhaskar and Mehta, 2010).

### 3.1.2 Proportion of particle size mass concentration

The concentration of particle matter fluctuated considerably during the observation period (shown in Fig. 2). The largest proportion of each month during the observation period was $PM_{2.5\text{-}10}$ (Fig. 3). The highest monthly average concentrations of $PM_{<1}$ and $PM_{1\text{-}2.5}$ were detected in January 2022, and the highest monthly average concentrations of $PM_{2.5\text{-}10}$ and $PM_{>10}$ were observed in March 2022. The percentage of $PM_{2.5}$ concentration in winter was higher than in other seasons, while $PM_{2.5\text{-}10}$ concentrations was higher in spring than in other seasons. This situation may be related to the strong windy in spring. Strong winds facilitated the dispersion of fine particle matter, while in winter, the conditions for the dispersion of fine particle matter were unfavorable, and heating emissions were more pronounced, resulting in a higher concentration of fine particle matter than in other seasons (Li *et al.*, 2020b). Compared with the studies of heavy pollution days caused by particles in Tianjin (December 2013–January 2014), Hangzhou (December 2013–January

https://doi.org/10.4209/aaqr.230127

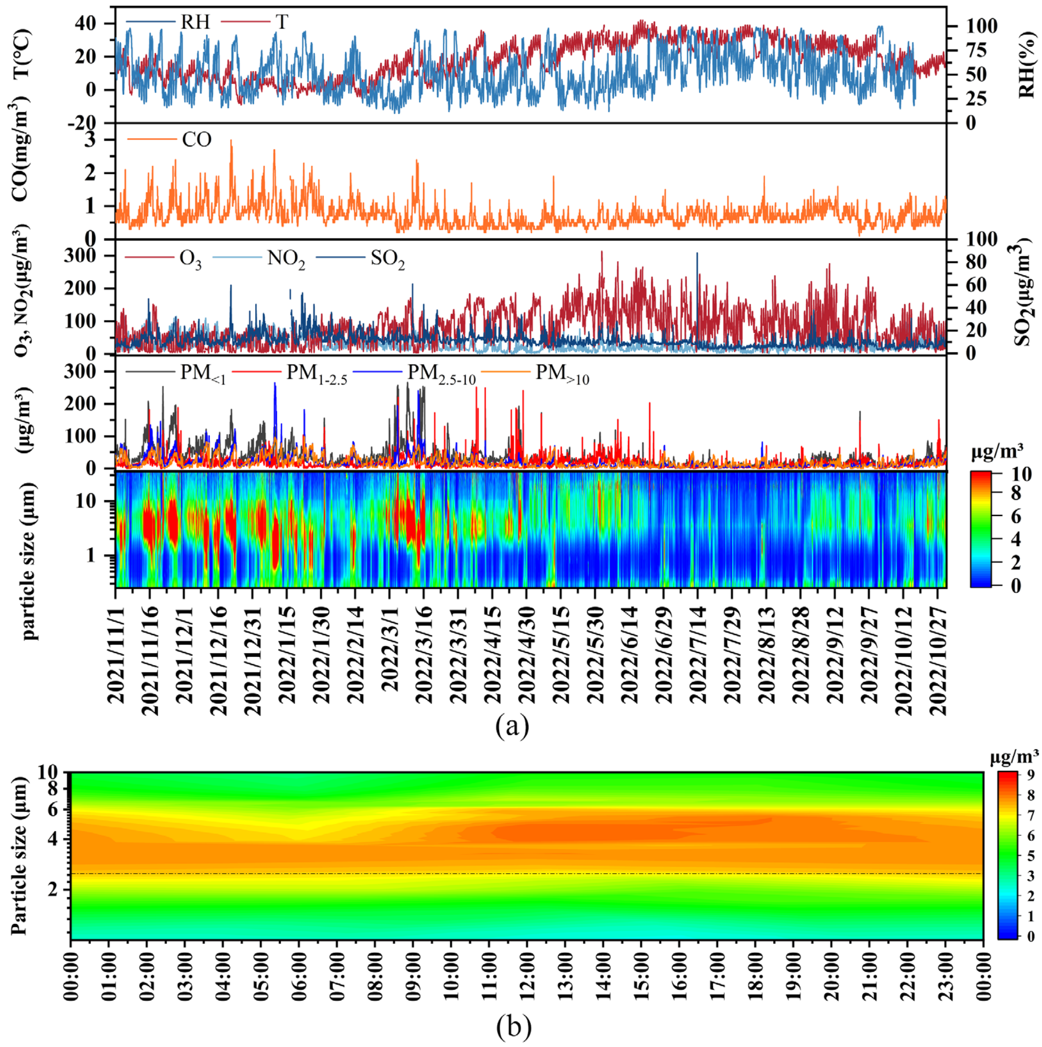


**Fig. 2.** Time series diagram of particle size concentration during winter 2021 to autumn 2022 in Jinan: (a) Meteorological conditions, gaseous pollutants, particle size distribution and particle concentration change from November 2021 to October 2022; (b) Daily variation of particle size concentration (mean value of observation time).

2014) and Chengdu (December 2013–January 2014) mentioned above, particle size distribution in Jinan showed similar characteristics during polluted process in winter.

## 3.2 Correlation Analysis of $PM_{2.5}$ with Meteorological and Pollution Factors

### 3.2.1 Pearson analysis and Single-factor model

To better show the effect factors related to particle size, data acquired in heavy polluted seasons (from November 1, 2021 to April 30, 2022) were collected for model analysis. The linear relationship could indicate the effect factors more effectively and it was more valuable for the environmental initiatives during polluted episode. The meteorological factors that correlate well with $PM_{2.5}$ were temperature (T), relative humidity (RH) and wind speed (WS); the pollution factors were CO, $NO_2$, $SO_2$, and $PM_{2.5-10}$. The factors that correlated better with $PM_{2.5-10}$ were CO and $SO_2$, and those correlated well with $PM_{>10}$ was $SO_2$. The correlation between temperature, wind speed, CO, $NO_2$ and particle size concentration decreases with the increasing particle size, and the correlation between $O_3$ and $PM_{2.5-10}$ was better than other particle size segments (Fig. 4).

The $PM_{2.5}$ concentration increased with temperature when the temperature was below 0°C and above 25°C observably (Fig. 5(a)). This may due to high temperature accelerates the translation from the precursors gas to $PM_{2.5}$ (Wang and Ogawa, 2015). Meanwhile, rising temperatures in winter often accompanied by a thicker inversion layer, leading to higher $PM_{2.5}$ concentration (Meriwether and Gardner, 2000). $PM_{2.5}$ was also significant positively correlated with relative humidity (RH) (Fig. 5(b)). The hygroscopic $PM_{2.5}$ increases its mass significantly as RH increases (Chen *et al.*, 2022). Meanwhile, A portion of volatile organic chemicals (VOCs) can react in the

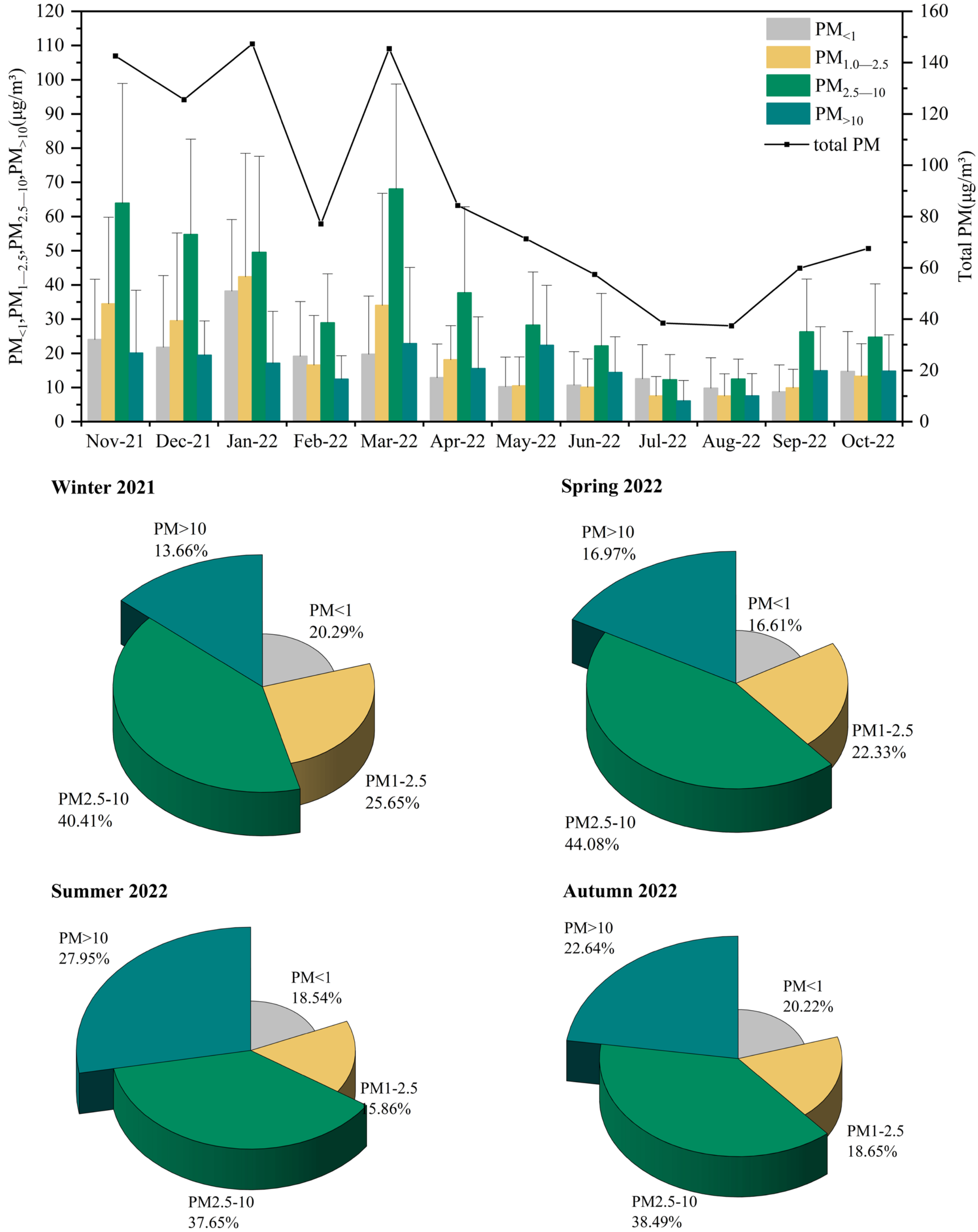


**Fig. 3.** Change in monthly average mass concentration of different particle sizes and its proportion in Jinan from winter 2021 to autumn 2022.

https://doi.org/10.4209/aaqr.230127

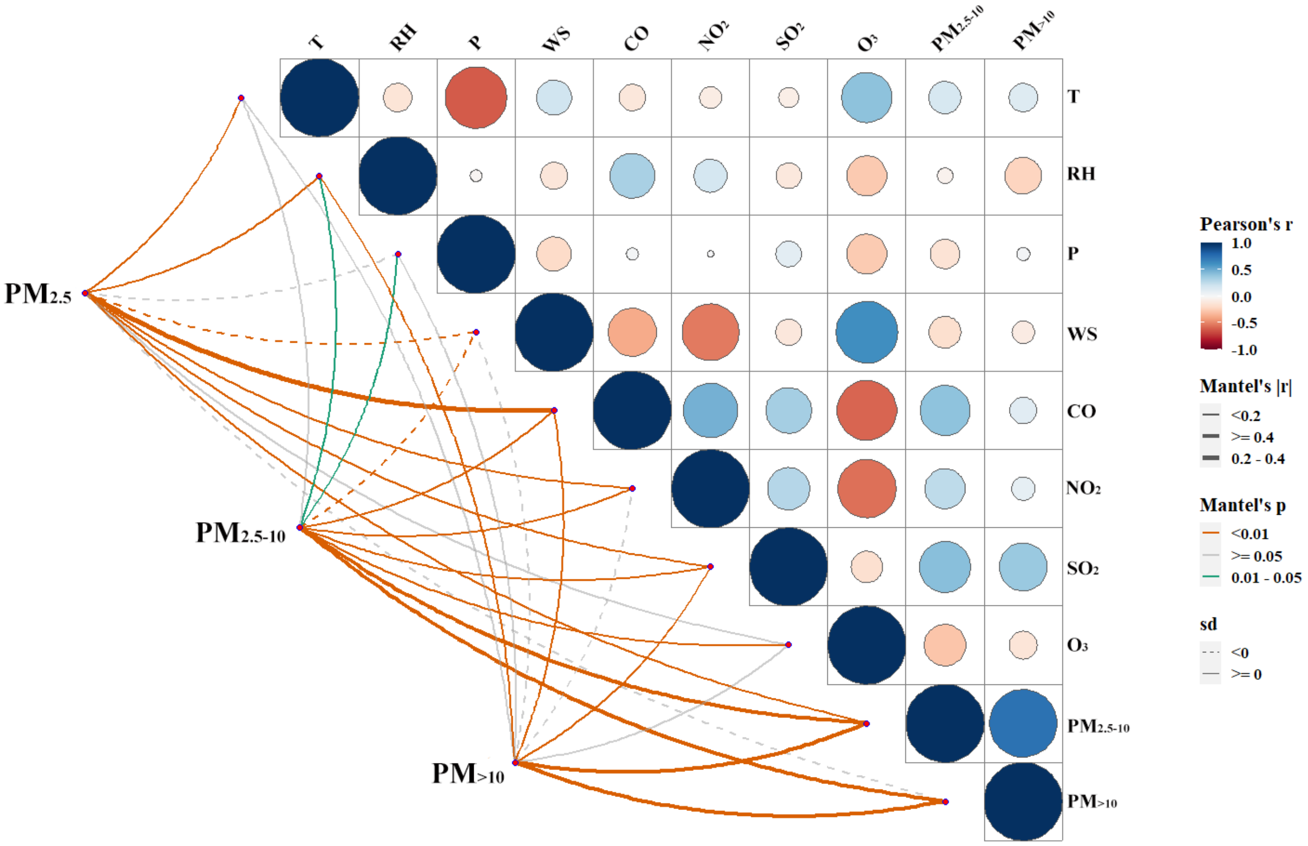


**Fig. 4.** Pearson correlation heat map of meteorological factors and air pollutants in the heavy polluted seasons: the left side shows the results of Mantel test, the thicker the line the larger the Mantel's r, the darker the color the larger Mantel's P, the solid line represents positive correlation, the dashed line represents negative correlation. The results of the Pearson test are shown on the right.

aqueous phase to formed secondary organic aerosol (SOA) (Sui *et al.*, 2021b). Nitrate and sulfate were transferred to higher size particle matters at high relative humidity more readily (Cheng *et al.*, 2015). Also, high relative humidity can aggravate particulate emissions from car engines (Zalakeviciute *et al.*, 2018). With the increase of wind speed, the $PM_{2.5}$ concentration showed a decreasing trend. This was due to low wind speed was not conducive to the diffusion of fine particles, and strong wind was one of the main factors for their diffusion (Fig. 5(d)) (Han *et al.*, 2016). The correlation coefficient between $PM_{2.5}$ and CO was large. CO is identified as a marker related to diffusion conditions and combustion sources. High CO concentration often indicates poor diffusion conditions or more emission from combustion sources, which favors the formation of fine particles, resulting in a consistent concentration trend of $PM_{2.5}$ and CO (Berglen *et al.*, 2004).

In the single-factor model, 10 environmental influencing factors were selected one at a time as explanatory variables. $PM_{2.5}$ was used as the response variable in order to construct the model for analyzing the degree of fit of each factor with $PM_{2.5}$ concentration (Table S1). The results showed that the p-values of each environmental factor were less than 0.001 and the degrees of freedom of each factor were greater than 1. It indicated that the 10 explanatory variables have a significant effect on $PM_{2.5}$ concentration during the observation period.

### 3.2.2 Multiple-factor model and influential effect

The influencing factors that passed the hypothesis test and were statistically significant in the single-factor model were used as explanatory variables in GAM in the multi-factor model. $PM_{2.5}$ concentration were used as the response variable and the model was constructed for fitting analysis (listed in Table S2). The results showed that in the multi-influence model, each factor with $P < 0.001$ and df $> 1$ passed the significance test, adjusted $R^2$ was 0.742, the total deviance

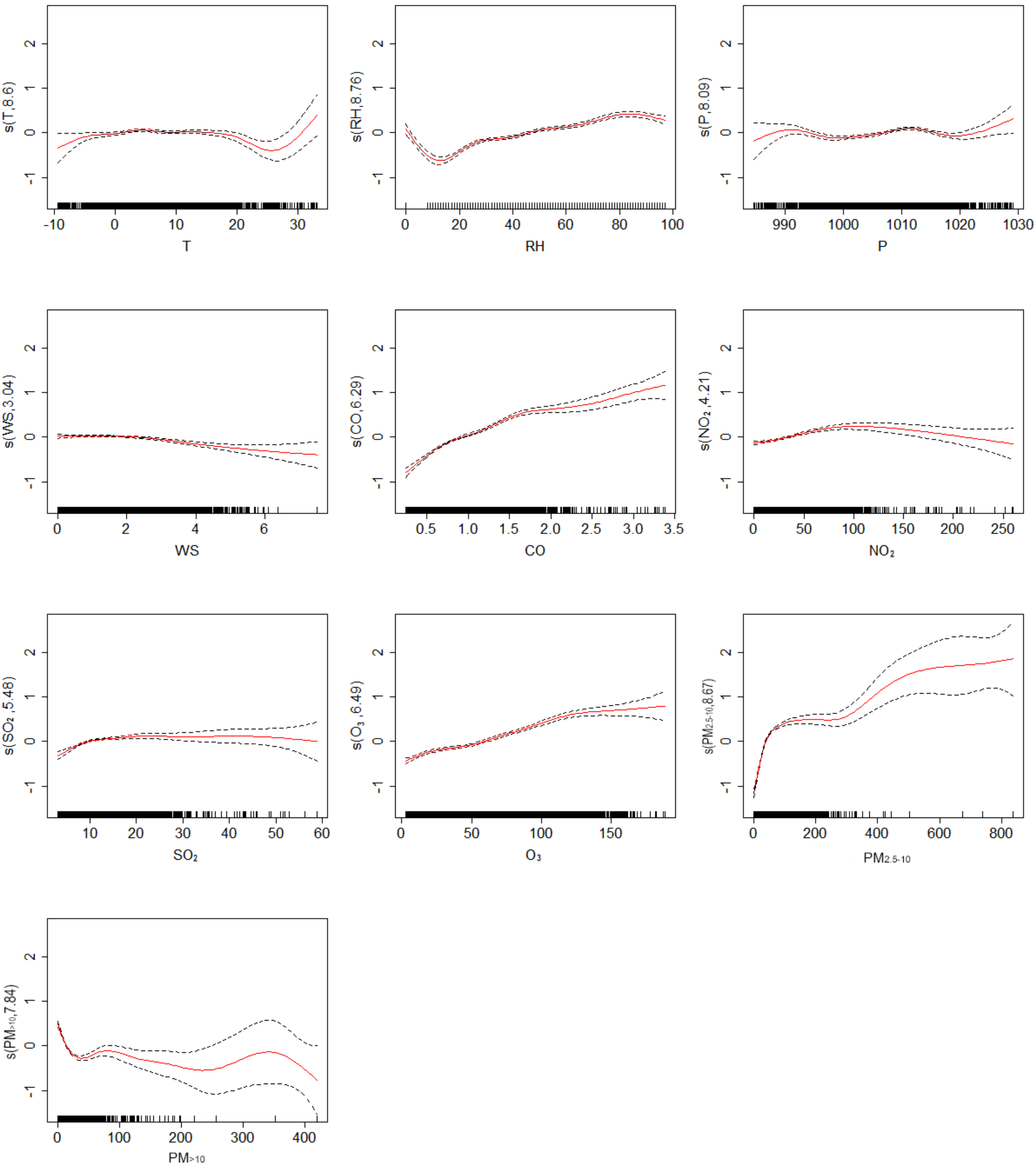


**Fig. 5.** Response curves of $PM_{2.5}$ concentration to changes in (a) air temperature, (b) relative humidity, (c) air pressure, (d) wind speed, (e) CO concentration, (f) $NO_2$ concentration, (g) $SO_2$ concentration, (h) $O_3$ concentration, (i) $PM_{2.5\text{-}10}$, and (j) $PM_{>10}$. The y-axis represents the smoothing function values and df is the degree of freedom for the trend. The x-axis represents the measured values of the influencing factor, the solid curve indicates the trend in $PM_{2.5}$ concentration with the change of influencing factors, and the broken line area that is centered around the solid line indicates the CI (lower and upper limits) of $PM_{2.5}$ concentration.

https://doi.org/10.4209/aaqr.230127

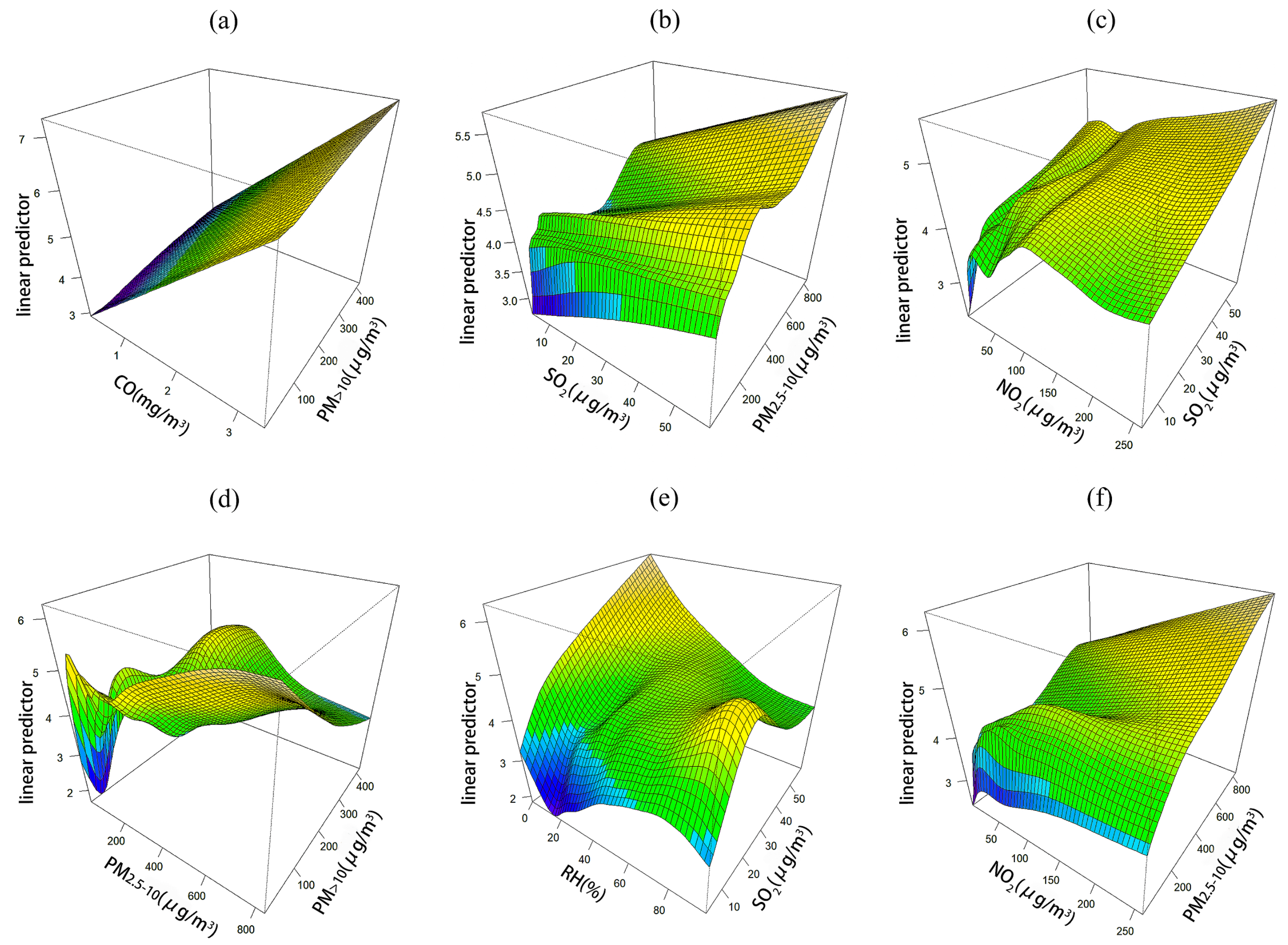


**Fig. 6.** Three-dimensional plots for the interaction effects of (a) CO and $PM_{>10}$, (b) $SO_2$ and $PM_{2.5\text{-}10}$, (c) $NO_2$ and $SO_2$, (d) $PM_{2.5\text{-}10}$ and $PM_{>10}$, (e) relative humidity and $SO_2$, (f) $NO_2$ and $PM_{2.5\text{-}10}$ on variations in $PM_{2.5}$ concentration in the heavy pollution process from November 2021 to October 2022 in Jinan.

explained was 74.7% (higher than that of the single-factor model) and AIC was 3748.665. The results showed that all 10 environmental impact factors significantly affected $PM_{2.5}$ concentration changes under the condition of *P*-value < 0.001, with some statistical significance and significant linear or non-linear relationships.

The smoothed regression functions of the explanatory variables were obtained by establishing GAM for the multi-factor model with $PM_{2.5}$ response variables. Then the effect map of each influence factor on $PM_{2.5}$ concentration was illustrated (Fig. 5). Moreover, a multi-factor GAM was conducted to evaluate the interaction effects of all the influencing factors on $PM_{2.5}$ concentration based on the single-factor mode. 12 of 45 interaction items were mapped that were significant and passed the statistical significance test (Fig. 6). During the sample period, all 12 interaction terms had high interpretation rates and variance contributions with *P*-value < 0.01 and *F*-value of 48.07–607.1. It indicated that these interaction terms fit better with $PM_{2.5}$ concentration, and the multi-factor model was better than the single-factor model in explaining $PM_{2.5}$ concentration changes and analyzing the interactions among the influencing factors. On the whole, the linear relationship between CO and $PM_{2.5}$ was the strongest, CO-$PM_{>10}$, CO-$NO_2$, P-CO, RH-CO, and $PM_{2.5}$ also had better interaction (seen in Table 1).

During the observation period, the strongest interactive species were CO, $PM_{>10}$ and $PM_{2.5}$. When CO concentration was certain, $PM_{2.5}$ concentration had a linear relationship with $PM_{>10}$ (Fig. 6(a)). In detail, when $PM_{2.5\text{-}10}$ concentrations were low, $PM_{2.5}$ concentration decreased

ORIGINAL RESEARCH
https://doi.org/10.4209/aaqr.230127

**Table 1.** Significant ($p < 0.01$) interaction terms (e.g., "P-CO" means the interaction effect of air pressure and CO) that mainly explained the variations in $PM_{2.5}$ concentration during the period of November 2021 to April 2022 in Jinan in the multi-factor GAM.

| Interaction term | CO-$PM_{>10}$ | CO-$NO_2$ | P-CO | RH-CO | CO-$SO_2$ | CO-$O_3$ |
|---|---|---|---|---|---|---|
| edf | 3.87 | 8.74 | 27.37 | 20.03 | 27.66 | 28.31 |
| Ref. df | 4.93 | 11.29 | 28.82 | 24.21 | 28.88 | 28.96 |
| *F*-value | 607.10 | 284.60 | 154.30 | 150.10 | 144.00 | 135.70 |
| *P*-value | < 2e-16*** | < 2e-16*** | < 2e-16*** | < 2e-16*** | < 2e-16*** | < 2e-16*** |
| Interaction term | $PM_{2.5-10}$-$PM_{>10}$ | WS–CO | $NO_2$-$PM_{2.5–10}$ | $SO_2$-$PM_{2.5–10}$ | $O_3$-$PM_{2.5–10}$ | $NO_2$-$SO_2$ |
| edf | 27.95 | 25.65 | 25.39 | 18.21 | 21.66 | 26.59 |
| Ref. df | 28.93 | 28.33 | 28.21 | 22.82 | 26.02 | 28.63 |
| *F*-value | 132.40 | 126.60 | 73.73 | 64.41 | 61.69 | 48.07 |
| *P*-value | < 2e-16*** | < 2e-16*** | < 2e-16*** | < 2e-16*** | < 2e-16*** | < 2e-16*** |

[1] This indicates $p < 0.001$.

sharply as $PM_{>10}$ increased, and increased with $NO_2$ and $SO_2$. This was because higher wind speed was conducive to $PM_{2.5}$ dispersion, however, it can trigger local dust raising caused higher TSP concentrations. When $PM_{2.5-10}$ concentrations were high, $PM_{2.5}$ was negatively correlated with $PM_{>10}$ concentrations and positively correlated with $NO_2$ and $SO_2$ concentrations (Figs. 6(b), 6(d), and 6(f)). $PM_{2.5}$ concentration increased and then decreased with $SO_2$ concentration when exposed to lower RH; there was a linear relationship between $SO_2$ and $PM_{2.5}$ concentration at higher RH, at $PM_{2.5}$ concentration reached the maximum when medium RH and high $SO_2$ concentration were observed (Fig. 6(e)). It was suggested both moisture absorption of $PM_{2.5}$ and $SO_2$ conversion in water vapor caused high $PM_{2.5}$ concentration (Yang *et al.*, 2015). In winter, high pressure usually means local region was controlled by cold air from the northwest with cleaner air mass. While low pressure was often accompanied by high RH, leading to higher $PM_{2.5}$ concentration (Jian *et al.*, 2012). The increasing temperature and RH were usually accompanied by thicker inversion layer. Meanwhile, high relative humidity favors the $PM_{2.5}$ hygroscopic process (Chen *et al.*, 2020). $PM_{2.5}$ and $SO_2$ concentrations were positively correlated when $NO_2$ concentrations were constant (Fig. 6(c)). Both $NO_2$ and $SO_2$ are important precursors of atmospheric particulate pollutants by forming $SO_3^{2-}$, $SO_4^{2-}$, $NO_3^-$, and $NO_2^-$ (Meng *et al.*, 2022). By constructing GAM for each influencing factor and analyzing the interaction, we found that the multi-factor model can better characterize the variation of $PM_{2.5}$ concentration under each influencing factor than the single-factor model. In summary, the multi-factor model and the interaction of influencing factors were a powerful tool in analyzing the characteristics of $PM_{2.5}$ concentration changes, and the simulations were closer to realistic conditions.

## 3.3 Possible Factors Contribute to Air Pollution

### 3.3.1 Heavily polluted processes

In order to evaluate particle size distribution in polluted episodes, two typical heavily polluted processes in winter (November 12, 2021, 0:00–November 22, 2021, 0:00) and spring (March 6, 2022, 0:00–March 13, 2022, 0:00) were selected based on the time distribution of particle concentration as shown in Fig. 2 and Fig. 7. The results showed that the heavily polluted process in winter was dominated by fine particle matter, with the main particle size was concentrated to $PM_{<1}$ and $PM_{1-2.5}$. While in spring the polluted episode was caused by coarse particle matter ($PM_{2.5-10}$ and $PM_{>10}$).

In winter 2021, $PM_{2.5-0}$ predominated at the beginning of the pollution phase, then gradually decreased. Meanwhile, $PM_{<1}$ and $PM_{1-2.5}$ increasing along with the pollution phase. Combined with the meteorological conditions, the higher wind speed favored local dust production. As the wind calm down, the diffusion starts to degrade results in the assembling of fine particles. In spring 2022, at the beginning of the pollution phase, the main particle matter was dominated by $PM_{2.5-10}$ and $PM_{>10}$; as the wind speed got stronger $PM_{2.5-10}$ and $PM_{>10}$ concentrations increased rapidly. While only slightly $PM_{1-2.5}$ increasing was observed. In the later polluted period, $PM_{2.5-10}$

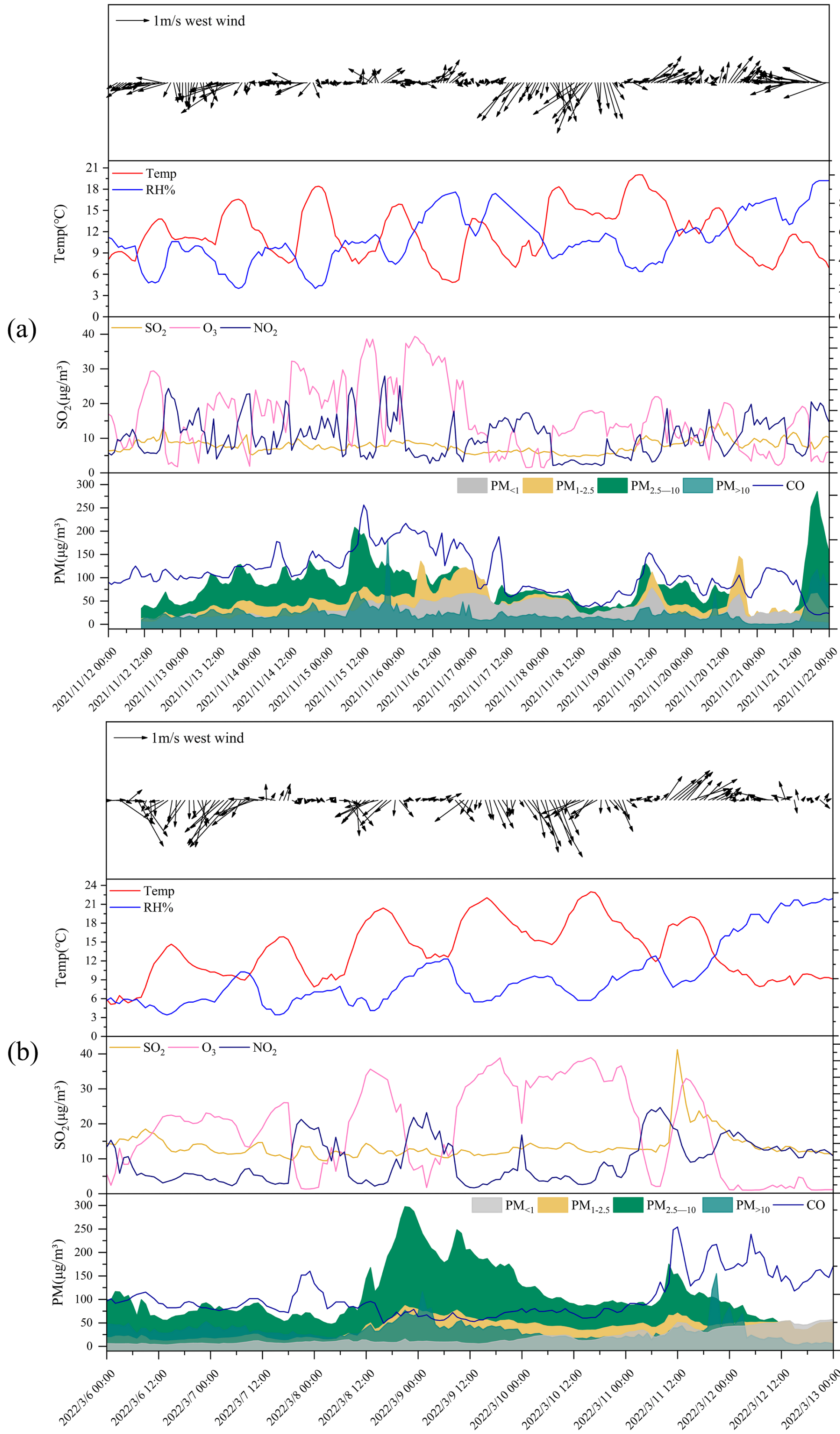


**Fig. 7.** Evolution of particle matters ($PM_{<1}$, $PM_{1\text{-}2.5}$, $PM_{2.5\text{-}10}$, $PM_{>10}$), gaseous pollutants (CO, $NO_2$, $SO_2$, and $O_3$) and meteorological parameter (Temperature, relative humidity, wind speed and wind direction, the arrow direction stands for wind angle) in (a) winter of 2021 and (b) spring of 2022 during heavy pollution.

and $PM_{>10}$ concentrations began to decrease and $PM_{<1}$ concentrations began to increase. This may due to the wind speed reduced in the later phase. Therefore, the concentrations of coarse particles decreases and the concentrations of fine particles increases. In most winter heavily polluted process, wind speed kept less than 2.0 m $s^{-1}$, relative humidity (RH) was higher than 60.0% and temperature was below 12.0°C. Such weather conditions was conducive to inversion layer formation and enhances pollution effects caused by local emissions (Akpinar *et al.*, 2008). Therefore, strictly controlling emissions should be adopted during such steady weathers, e.g., the restriction of motor vehicle driving, fuel gas recovery at gas stations, and emission controls in the petroleum and paint industries which can help reduce the precursors of PM such as $NO_2$, $SO_2$, and VOCs.

### 3.3.2 Long-range transport

Besides local emission, long-range transport was also found as an important source that contributes to particle pollution. A total of 2146 trajectories were identified in winter 2021. In winter, particle matter pollution in Jinan was primarily attributed to short-range transport, with transport heights mainly ranging from near the surface (0–600 m, seen in Fig. 8(a)). These trajectories were aggregated into 6 trajectory types by clustering analysis. The largest proportion was Trajectory 2 (29.08%), which mainly come from the short-range transmission in the northern region. Trajectory 6 (24.56%) and Trajectory 1 (20.62%) mainly come from the short-range transmission in the southwest and southern region, respectively. While Trajectory 5 (15.66%) mainly come from the eastern coastal transmission and Trajectory 3 (9.37%) come from the long-range transmission in the northwest. Particle matter pollution in spring was dominated by medium-range and long-range transport (height 600–800 m, listed in Fig. 8(b)) with 2,136 trajectories. Compared to winter, air mass in spring was dominated by long-range transport, with the largest proportion of Trajectory 3 (21.96%) come from the southwest. This was followed by Trajectory 5 (18.36%) come from the southeast. Long-range transported air masses come from the northwest and northeast regions increased and short-range transport decreased compared to winter. Long-distance transport from the north (600–1200 m) was generally situated above the boundary layer, and the air masses were relatively clean. In contrast, short-distance transport (0–400 m) often occurred below the boundary layer and was more susceptible to the influence of ground pollutants and locally generated pollution.

The statistical results of pollution trajectories showed that the particulate pollution during winter 2021 to autumn 2022 in Jinan was mainly influenced by trajectories come from the eastern coastal region and the southeast region. $PM_{2.5}$, $PM_{10}$ and $PM_{2.5\text{-}10}$ in winter were mainly transported from the north (Trajectory 2) and east (Trajectory 5) while $PM_{>10}$ were mainly from the north (Trajectory 2) and southwest (Trajectory 6). PM in spring were mainly from the northeast (Trajectory 1) and southeast (Trajectory 5). In addition, $PM_{2.5}$ was also more influenced by the northeast proximity transport (Trajectory 2) (Table 2). $PM_{2.5}$ and $PM_{10}$ in summer were mainly from the northeast (Trajectory 3) and southwest (Trajectory 6) while in the autumn were mainly from the southwest (Trajectory 6) and $PM_{10}$ were mainly from the south (Trajectory 5) (Table S3). The pollution trajectories were much less in summer and autumn than in winter and spring as summarized in Table 2 and Fig. 8. Besides local emission, long-range transport was also found as an significant factor that contributes to urban air pollution (Huang *et al.*, 2014). The potential source region of $PM_{2.5}$ and $PM_{10}$ in Jinan in winter and spring indicated $PM_{2.5}$ and $PM_{10}$ were mainly come from short-range transmission in winter and long-range transmission in spring (Fig. 9).

$PM_{2.5}$ was mainly influenced by the southeastern Bohai region in winter, while mainly transported from the northeast in spring. The major transport source of $PM_{10}$ was northern and eastern short-range transport in winter, while in spring, air masses from the northeastern coastal and southwestern regions were the main transport $PM_{10}$ sources. It could be found that particles in winter were mainly dominated by local emissions and short-range transport. The dispersion conditions were worse in winter, while in spring the long-range transport become an important transmission mode (Sui *et al.*, 2021a). Based on the correlation analysis, during the winter 2021, the passage of cold air from north led to a decrease in temperature, thereby favor the diffusion of particles. As seen in Table 2, air masses originating from the northern regions were relatively

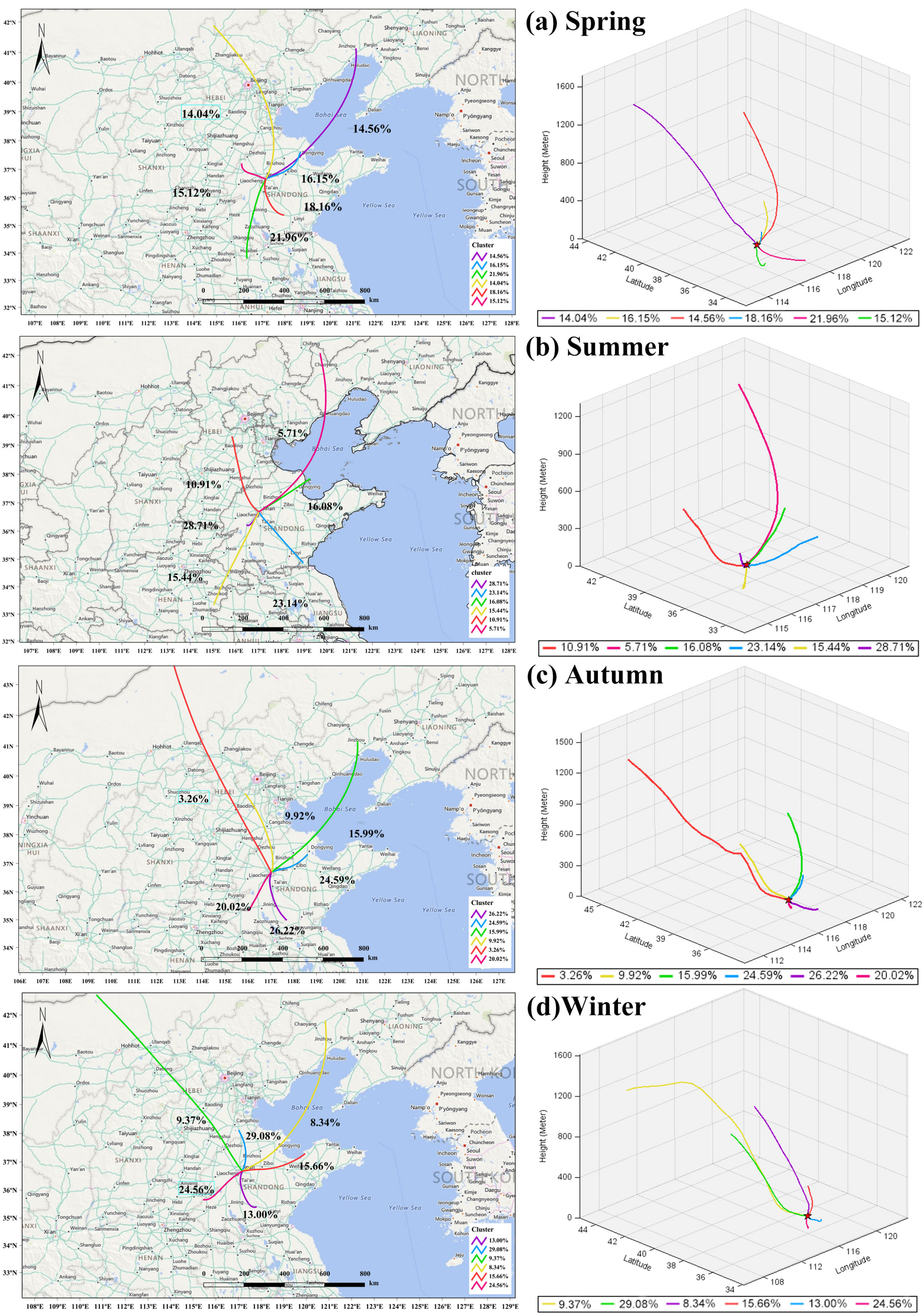


**Fig. 8.** Result of cluster analysis of backward trajectory of airflow in Jinan in (a) winter 2021, (b) spring, (c) summer, and (d) autumn 2022.

**Table 2.** Polluted trajectory transmission statistics in winter 2021 and spring 2022.

| PM | Winter 2021 | | | | Spring 2022 | | |
|---|---|---|---|---|---|---|---|
| | Cluster | P_Number | P_Mean_Val | P_Stdev | P_Number | P_Mean_Val | P_Stdev |
| $PM_{2.5}$ | 1 | 55 | 106.15 | 20.44 | 146 | 86.38 | 44.49 |
| | 2 | 257 | 120.53 | 31.32 | 198 | 73.80 | 27.11 |
| | 3 | 15 | 107.66 | 28.53 | 264 | 52.83 | 16.35 |
| | 4 | 67 | 118.25 | 28.42 | 112 | 51.53 | 14.58 |
| | 5 | 185 | 134.19 | 58.99 | 228 | 65.66 | 21.73 |
| | 6 | 126 | 102.92 | 15.25 | 122 | 62.99 | 28.09 |
| | All | 705 | 119.35 | 39.43 | 1070 | 65.04 | 28.54 |
| $PM_{10}$ | 1 | 91 | 218.02 | 66.81 | 96 | 246.97 | 76.24 |
| | 2 | 353 | 252.52 | 72.79 | 87 | 220.66 | 55.03 |
| | 3 | 30 | 212.92 | 64.51 | 58 | 200.54 | 52.53 |
| | 4 | 83 | 230.12 | 60.86 | 47 | 253.75 | 124.36 |
| | 5 | 221 | 281.32 | 103.92 | 148 | 209.99 | 40.99 |
| | 6 | 165 | 215.25 | 45.86 | 62 | 201.76 | 49.24 |
| | All | 943 | 246.19 | 79.70 | 498 | 220.99 | 67.38 |
| $PM_{2.5-10}$ | 1 | 47 | 99.63 | 28.89 | 108 | 91.48 | 41.48 |
| | 2 | 178 | 106.12 | 23.94 | 48 | 84.62 | 43.05 |
| | 3 | 34 | 123.22 | 55.03 | 76 | 97.92 | 60.32 |
| | 4 | 41 | 96.12 | 16.37 | 70 | 117.19 | 66.32 |
| | 5 | 127 | 115.85 | 33.20 | 141 | 109.58 | 65.75 |
| | 6 | 102 | 89.94 | 15.06 | 87 | 89.00 | 42.99 |
| | All | 529 | 105.08 | 29.72 | 530 | 99.58 | 56.28 |
| $PM_{>10}$ | 1 | 50 | 37.39 | 25.84 | 93 | 34.78 | 14.32 |
| | 2 | 177 | 35.60 | 11.07 | 48 | 39.34 | 27.76 |
| | 3 | 51 | 50.46 | 28.62 | 75 | 37.41 | 15.88 |
| | 4 | 31 | 34.89 | 11.15 | 97 | 50.60 | 40.73 |
| | 5 | 94 | 41.83 | 19.47 | 131 | 39.60 | 29.80 |
| | 6 | 123 | 32.10 | 11.16 | 86 | 30.20 | 11.64 |
| | All | 526 | 37.46 | 17.69 | 530 | 38.91 | 26.85 |

clean, and their contribution to particulate pollution was comparatively minor. Otherwise, higher temperatures in winter indicated stable boundary layer thus the pollution from fine particle matter may have been exacerbated. Therefore, local emissions and short-range transport from the southwest and northern regions were the main modes of particle r transport during the winter. In contrast, meteorological in spring was often characterized by high wind speeds, low humidity, and rising temperatures, creating favorable conditions for the particle transported from the northern areas. In summary, the potential source areas suggested particle matter were mainly transported from the north industrial cities, the northwest Loess Plateau and Inner Mongolia region with low vegetation cover and serious land desertification and the southwest Central Plains with serious industrial pollution (Li *et al.*, 2021).

## 4 CONCLUSIONS

The results showed that the main particle size distribution in Jinan was 1.0–13.0 µm, in winter, PM was dominated by secondary pollutants and fine particles, the main particle size distribution was $PM_{<1}$ and $PM_{1-2.5}$. In spring, coarse particles occupied most PM, while in clean days a large proportion of PM was fine particles. In summer and autumn, particle matter pollution was lighter, with the main particle size was $PM_{2.5-10}$. From the daily variation, particle pollution reached peaks at 7:00–12:00 and 17:00–1:00. This may be associated with vehicle emissions, vehicle brake wear, human activity emissions in the morning and the adverse layer effects at night.

Pearson and GAM analysis showed that temperature, RH, wind speed, $NO_2$ and $SO_2$ concentrations

https://doi.org/10.4209/aaqr.230127

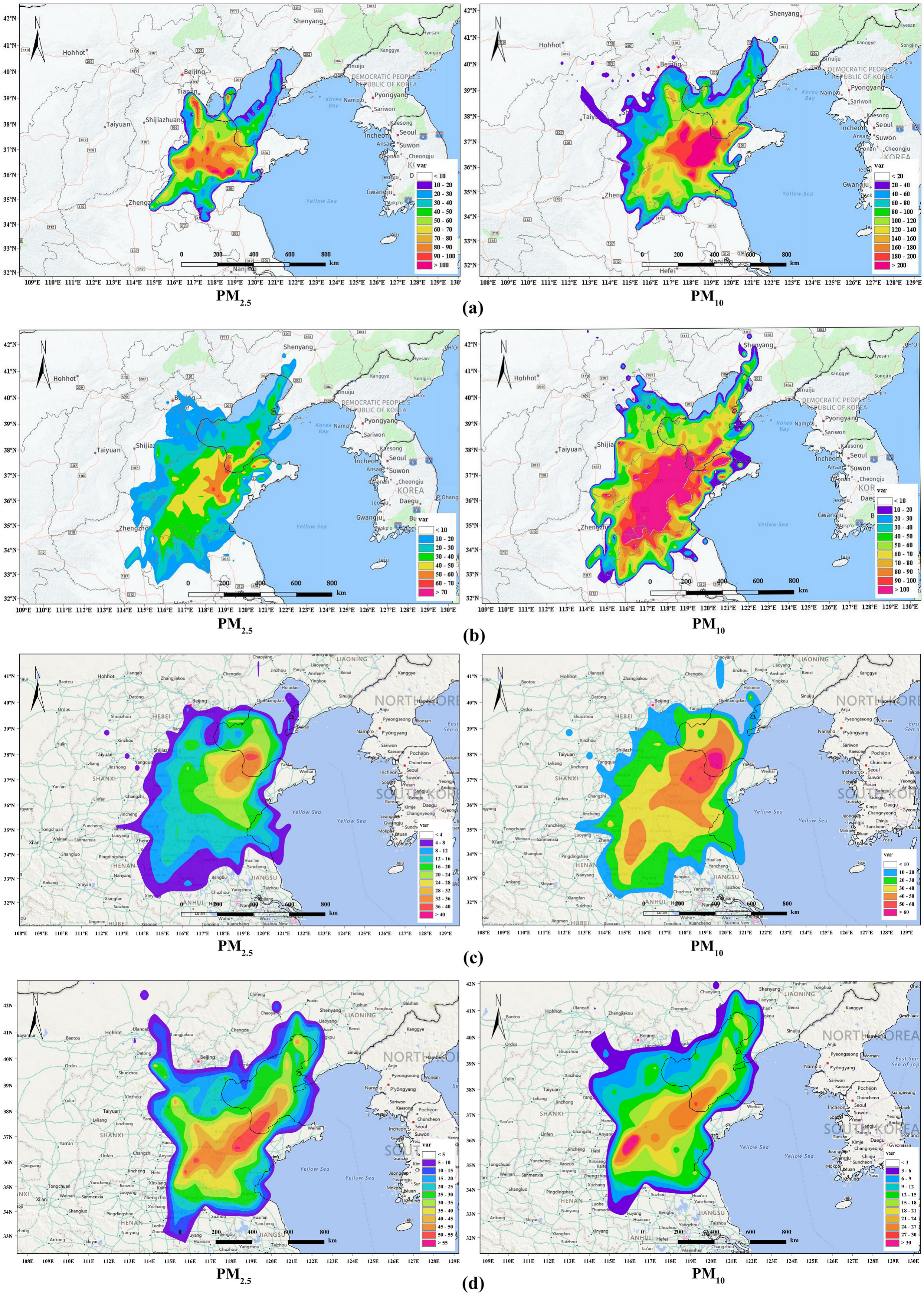


**Fig. 9.** The CWT analysis for $PM_{2.5}$ and $PM_{10}$ in Jinan in (a) winter 2021, (b) spring, (c) summer, and (d) autumn 2022.

had significant effects on fine particle matter concentrations. $PM_{2.5}$ concentration were positively correlated with RH, CO, $NO_2$, $SO_2$, and $PM_{2.5-10}$ concentrations, while negatively correlated with wind speed, $O_3$ and $PM_{>10}$ concentrations. The correlation between temperature, wind speed, CO, $NO_2$ and particle size concentration decreased with the increasing particle size. $PM_{2.5-10}$ was found to be positively correlated with gaseous pollutants such as $NO_2$, $SO_2$, and CO, as well as RH and air pressure. Besides, $PM_{>10}$ was positively associated with CO, $SO_2$, and RH, but negatively correlated with $NO_2$ and wind speed. The interaction between meteorological factors and air pollutants also showed a strong correlation with PM concentrations. The hygroscopicity of PM caused a significant mass increase as the RH increased. High RH also aggravated the particle matter emissions from automobile engines. The analysis of backward trajectories and concentration weighted trajectory (CWT) showed that besides local source, particle matter pollution in Jinan mainly came from the eastern coastal region and the southeastern region. Winter and spring were more influenced by regional distance transport. In winter, $PM_{2.5}$, $PM_{2.5-10}$, and $PM_{10}$ were mainly transported from the east and north while $PM_{>10}$ was mainly from the north and southwest. In spring, PM was mainly transported from the northeast southeast and the close transmission from the northeast.

In general, the treatment of particle matter pollution should be focused on the winter and spring, and the emission controls on $NO_2$ would be essential to reduce fine particle pollution in the next phases. Also, more stringent emission control under low temperature together with high RH should be issued. The control of primary and coarse particle matter (e.g., road and construction dust) should be a primary measure when the strong windy appeared in spring. To improve air quality for a long-term, the development of stricter motor vehicle emission standards, fuel gas recovery at gas stations, and emission controls of the oil and paint industries would help reduce the precursors of fine particles such as $NO_2$, $SO_2$, and VOCs. Moreover, regional cooperation is essential to mitigate urban particle pollution from regional scale.

## ACKNOWLEDGMENTS

This research was financed by Natural Science Foundation of Shandong Province of China project (ZR2022QB137).

## DISCLAIMER

Reference to any companies or specific commercial products does not constitute conflict of interest.

## SUPPLEMENTARY MATERIAL

Supplementary material for this article can be found in the online version at https://doi.org/10.4209/aaqr.230127

## REFERENCES

Akpinar, S., Oztop, H.F., Kavak Akpinar, E. (2008). Evaluation of relationship between meteorological parameters and air pollutant concentrations during winter season in Elazığ, Turkey. Environ. Monit. Assess. 146, 211–224. https://doi.org/10.1007/s10661-007-0073-9

Allen, A.G., Nemitz, E., Shi, J.P., Harrison, R.M., Greenwood, J.C. (2001). Size distributions of trace metals in atmospheric aerosols in the United Kingdom. Atmos. Environ. 35, 4581–4591. https://doi.org/10.1016/S1352-2310(01)00190-X

Berglen, T.F., Berntsen, T.K., Isaksen, I.S.A., Sundet, J.K. (2004). A global model of the coupled sulfur/oxidant chemistry in the troposphere: The sulfur cycle. J. Geophys. Res. 109, 2003JD003948. https://doi.org/10.1029/2003JD003948

Bhaskar, B.V., Mehta, V.M. (2010). Atmospheric particulate pollutants and their relationship with

meteorology in Ahmedabad. Aerosol Air Qual. Res. 10, 301–315. https://doi.org/10.4209/aaqr.2009.10.0069
Chen, L., Zhang, F., Zhang, D., Wang, X., Song, W., Liu, J., Ren, J., Jiang, S., Li, X., Li, Z. (2022). Measurement report: Hygroscopic growth of ambient fine particles measured at five sites in China. Atmos. Chem. Phys. 22, 6773–6786. https://doi.org/10.5194/acp-22-6773-2022
Chen, Y., Xie, S., Luo, B., Zhai, C. (2014). Characteristics and origins of carbonaceous aerosol in the Sichuan Basin, China. Atmos. Environ. 94, 215–223. https://doi.org/10.1016/j.atmosenv.2014.05.037
Chen, Z., Chen, D., Zhao, C., Kwan, M., Cai, J., Zhuang, Y., Zhao, B., Wang, X., Chen, B., Yang, J., Li, R., He, B., Gao, B., Wang, K., Xu, B. (2020). Influence of meteorological conditions on $PM_{2.5}$ concentrations across China: A review of methodology and mechanism. Environ. Int. 139, 105558. https://doi.org/10.1016/j.envint.2020.105558
Cheng, Y., He, K., Du, Z., Zheng, M., Duan, F., Ma, Y. (2015). Humidity plays an important role in the $PM_{2.5}$ pollution in Beijing. Environ. Pollut. 197, 68–75. https://doi.org/10.1016/j.envpol.2014.11.028
Chuang, K.J., Yan, Y.H., Chiu, S.Y., Cheng, T.J. (2011). Long-term air pollution exposure and risk factors for cardiovascular diseases among the elderly in Taiwan. Occup. Environ. Med. 68, 64–68. https://doi.org/10.1136/oem.2009.052704
Deng, J., Du, K., Wang, K., Yuan, C.S., Zhao, J. (2012). Long-term atmospheric visibility trend in Southeast China, 1973–2010. Atmos. Environ. 59, 11–21. https://doi.org/10.1016/j.atmosenv.2012.05.023
Fu, G.Q., Xu, W.Y., Yang, R.F., Li, J.B., Zhao, C.S. (2014). The distribution and trends of fog and haze in the North China Plain over the past 30 years. Atmos. Chem. Phys. 14, 11949–11958. https://doi.org/10.5194/acp-14-11949-2014
Gao, Y., Lee, S.C., Huang, Y., Chow, J.C., Watson, J.G. (2016). Chemical characterization and source apportionment of size-resolved particles in Hong Kong sub-urban area. Atmos. Res. 170, 112–122. https://doi.org/10.1016/j.atmosres.2015.11.015
Han, L., Zhou, W., Li, W. (2016). Fine particulate ($PM_{2.5}$) dynamics during rapid urbanization in Beijing, 1973–2013. Sci. Rep. 6, 23604. https://doi.org/10.1038/srep23604
He, X., Lin, Z.S. (2017). Interactive effects of the influencing factors on the changes of $PM_{2.5}$ concentration based on GAM model. Huan Jing Ke Xue 38, 22–32. https://doi.org/10.13227/j.hjkx.201606061 (in Chinese)
Huang, R.J., Zhang, Y., Bozzetti, C., Ho, K.F., Cao, J.J., Han, Y., Daellenbach, K.R., Slowik, J.G., Platt, S.M., Canonaco, F., Zotter, P., Wolf, R., Pieber, S.M., Bruns, E.A., Crippa, M., Ciarelli, G., Piazzalunga, A., Schwikowski, M., Abbaszade, G., Schnelle-Kreis, J., *et al.* (2014). High secondary aerosol contribution to particulate pollution during haze events in China. Nature 514, 218–222. https://doi.org/10.1038/nature13774
Huang, X.G., Shao, T.J., Zhao, J.B., Cao, J.J., Lü, X.H. (2020). Influencing factors of ozone concentration in Xi'an based on generalized additive models. Huan Jing Ke Xue 41, 1535–1543. https://doi.org/10.13227/j.hjkx.201906067 (in Chinese)
Jian, L., Zhao, Y., Zhu, Y.P., Zhang, M.B., Bertolatti, D. (2012). An application of ARIMA model to predict submicron particle concentrations from meteorological factors at a busy roadside in Hangzhou, China. Sci. Total Environ. 426, 336–345. https://doi.org/10.1016/j.scitotenv.2012.03.025
Karanasiou, A.A., Sitaras, I.E., Siskos, P.A., Eleftheriadis, K. (2007). Size distribution and sources of trace metals and n-alkanes in the Athens urban aerosol during summer. Atmos. Environ. 41, 2368–2381. https://doi.org/10.1016/j.atmosenv.2006.11.006
Li, B., Zhou, Z., Xue, Z., Wei, P., Ren, Y., Cao, L., Feng, X., Yao, Q., Ma, J., Xu, P., Chen, X. (2020a). Study on the pollution characteristics and sources of ozone in typical Loess Plateau city. Atmosphere 11, 655. https://doi.org/10.3390/atmos11060555
Li, C., Liu, M., Hu, Y., Zhou, R., Huang, N., Wu, W., Liu, C. (2020b). Spatial distribution characteristics of gaseous pollutants and particle matter inside a city in the heating season of Northeast China. Sustainable Cities Soc. 61, 102302. https://doi.org/10.1016/j.scs.2020.102302
Li, K., Chen, L., White, S.J., Han, K., Lv, B., Bao, K., Wu, X., Gao, X., Azzi, M., Cen, K. (2017a). Effect

of nitrogen oxides (NO and $NO_2$) and toluene on $SO_2$ photooxidation, nucleation and growth: A smog chamber study. Atmos. Res. 192, 38–47. https://doi.org/10.1016/j.atmosres.2017.03.017
Li, R., Wang, J., Xue, K., Fang, C. (2021). Spatial and temporal distribution characteristics and influencing factors analysis of particle matter pollution in Jinan City. Air Qual. Atmos. Health 14, 1267–1278. https://doi.org/10.1007/s11869-021-01015-9
Li, S., Zhai, L., Zou, B., Sang, H., Fang, X. (2017b). A generalized additive model combining principal component analysis for $PM_{2.5}$ concentration estimation. ISPRS Int. J. Geo-Inf. 6, 248. https://doi.org/10.3390/ijgi6080248
Lin, X., Liao, Y., Hao, Y. (2018). The burden associated with ambient $PM_{2.5}$ and meteorological factors in Guangzhou, China, 2012–2016: A generalized additive modeling of temporal years of life lost. Chemosphere 212, 705–714. https://doi.org/10.1016/j.chemosphere.2018.08.129
Liu, Y., Paciorek, C.J., Koutrakis, P. (2009). Estimating regional spatial and temporal variability of $PM_{2.5}$ concentrations using satellite data, meteorology, and land use information. Environ. Health Perspect. 117, 886–892. https://doi.org/10.1289/ehp.0800123
Liu, Y., Zhao, N., Vanos, J.K., Cao, G. (2017). Effects of synoptic weather on ground-level $PM_{2.5}$ concentrations in the United States. Atmos. Environ. 148, 297–305. https://doi.org/10.1016/j.atmosenv.2016.10.052
Ly, B.T., Matsumi, Y., Vu, T.V., Sekiguchi, K., Nguyen, T.T., Pham, C.T., Nghiem, T.D., Ngo, I.H., Kurotsuchi, Y., Nguyen, T.H., Nakayama, T. (2021). The effects of meteorological conditions and long-range transport on $PM_{2.5}$ levels in Hanoi revealed from multi-site measurement using compact sensors and machine learning approach. J. Aerosol Sci. 152, 105716. https://doi.org/10.1016/j.jaerosci.2020.105716
Ma, Y., Ma, B., Jiao, H., Zhang, Y., Xin, J., Yu, Z. (2020). An analysis of the effects of weather and air pollution on tropospheric ozone using a generalized additive model in Western China: Lanzhou, Gansu. Atmos. Environ. 224, 117342. https://doi.org/10.1016/j.atmosenv.2020.117342
Malandrino, M., Casazza, M., Abollino, O., Minero, C., Maurino, V. (2016). Size resolved metal distribution in the PM matter of the city of Turin (Italy). Chemosphere 147, 477–489. https://doi.org/10.1016/j.chemosphere.2015.12.089
Meng, F., Zhang, Y., Kang, J., Heal, M.R., Reis, S., Wang, M., Liu, L., Wang, K., Yu, S., Li, P., Wei, J., Hou, Y., Zhang, Y., Liu, X., Cui, Z., Xu, W., Zhang, F. (2022). Trends in secondary inorganic aerosol pollution in China and its responses to emission controls of precursors in wintertime. Atmos. Chem. Phys. 22, 6291–6308. https://doi.org/10.5194/acp-22-6291-2022
Meriwether, J.W., Gardner, C.S. (2000). A review of the mesosphere inversion layer phenomenon. J. Geophys. Res. 105, 12405–12416. https://doi.org/10.1029/2000JD900163
Moustafa, M., Mohamed, A., Ahmed, A.R., Nazmy, H. (2015). Mass size distributions of elemental aerosols in industrial area. J. Adv. Res. 6, 827–832. https://doi.org/10.1016/j.jare.2014.06.006
Norman, K.D. (2000). Applied regression analysis bibliography update. Commun. Stat.- Theory Methods 29, 2313–2341. https://doi.org/10.1080/03610920008832608
Parmar, R.S., Satsangi, G.S., Kumari, M., Lakhani, A., Srivastava, S.S., Prakash, S. (2001). Study of size distribution of atmospheric aerosol at Agra. Atmos. Environ. 35, 693–702. https://doi.org/10.1016/S1352-2310(00)00317-4
Qiao, L., Gao, L., Liu, Y., Huang, D., Li, D., Zheng, M. (2022). Recognition and health impacts of organic pollutants with significantly different proportions in the gas phase and size-fractionated particulate phase in ambient air. Environ. Sci. Technol. 56, 7153–7162. https://doi.org/10.1021/acs.est.1c08829
Shah, A.S.V., Langrish, J.P., Nair, H., McAllister, D.A., Hunter, A.L., Donaldson, K., Newby, D.E., Mills, N.L. (2013). Global association of air pollution and heart failure: a systematic review and meta-analysis. Lancet 382, 1039-1048. https://doi.org/10.1016/S0140-6736(13)60898-3
Sorek-Hamer, M., Strawa, A.W., Chatfield, R.B., Esswein, R., Cohen, A., Broday, D.M. (2013). Improved retrieval of $PM_{2.5}$ from satellite data products using non-linear methods. Environ. Pollut. 182, 417–423. https://doi.org/10.1016/j.envpol.2013.08.002
Sui, X., Qi, K., Nie, Y., Ding, N., Shi, X., Wu, X., Zhang, Q., Wang, W. (2021a). Air quality and public health risk assessment: A case study in a typical polluted city, North China. Urban Clim. 36, 100796. https://doi.org/10.1016/j.uclim.2021.100796

Sui, X., Xu, B., Yao, J., Kostko, O., Ahmed, M., Yu, X.Y. (2021b). New insights into secondary organic aerosol formation at the air–liquid interface. J. Phys. Chem. Lett. 12, 324–329. https://doi.org/10.1021/acs.jpclett.0c03319

Tan, J., Duan, J., Zhen, N., He, K., Hao, J. (2016). Chemical characteristics and source of size-fractionated atmospheric particle in haze episode in Beijing. Atmos. Res. 167, 24–33. https://doi.org/10.1016/j.atmosres.2015.06.015

Thurston, S.W., Wand, M.P., Wiencke, J.K. (2000). Negative binomial additive models. Biometrics 56, 139–144. https://doi.org/10.1111/j.0006-341X.2000.00139.x

Tian, S., Liu, Y., Wang, J., Wang, J., Hou, L., Lv, B., Wang, X., Zhao, X., Yang, W., Geng, C., Han, B., Bai, Z. (2020). Chemical compositions and source analysis of $PM_{2.5}$ during autumn and winter in a heavily polluted city in China. Atmosphere 11, 336. https://doi.org/10.3390/atmos11040336

Verbeke, T. (2007). Generalized additive models: an introduction with R. J. R. Stat. Soc. A 170, 262–262. https://doi.org/10.1111/j.1467-985X.2006.00455_15.x

Wang, H., Li, J., Peng, Y., Zhang, M., Che, H., Zhang, X. (2019). The impacts of the meteorology features on $PM_{2.5}$ levels during a severe haze episode in central-east China. Atmos. Environ. 197, 177–189. https://doi.org/10.1016/j.atmosenv.2018.10.001

Wang, J., Ogawa, S. (2015). Effects of meteorological conditions on $PM_{2.5}$ concentrations in Nagasaki, Japan. IJERPH 12, 9089–9101. https://doi.org/10.3390/ijerph120809089

Wang, J., Zhang, J., Liu, Z., Wu, J., Zhang, Y., Han, S., Zheng, X., Zhou, L., Feng, Y., Zhu, T. (2017). Characterization of chemical compositions in size-segregated atmospheric particles during severe haze episodes in three mega-cities of China. Atmos. Res. 187, 138–146. https://doi.org/10.1016/j.atmosres.2016.12.004

Wang, N., Li, N., Liu, Z., Evans, E. (2016). Investigation of chemical reactivity and active components of ambient VOCs in Jinan, China. Air Qual. Atmos. Health 9, 785–793. https://doi.org/10.1007/s11869-015-0380-1

Wang, X.F., Wang, W.X., Gao, X.M., Nie, W., Yu, Y.C., Yang, L.X., Chen, J.M. (2014). Characteristics and implications of aerosol mass size distributions in typical cities and mountain in China. Abstracts of Papers of the American Chemical Society 247.

Wei, N., Jia, Z., Men, Z., Ren, C., Zhang, Y., Peng, J., Wu, L., Wang, T., Zhang, Q., Mao, H. (2022). Machine learning predicts emissions of brake wear $PM_{2.5}$: model construction and interpretation. Environ. Sci. Technol. Lett. https://doi.org/10.1021/acs.estlett.2c00117

Westervelt, D.M., Horowitz, L.W., Naik, V., Tai, A.P.K., Fiore, A.M., Mauzerall, D.L. (2016). Quantifying $PM_{2.5}$-meteorology sensitivities in a global climate model. Atmos. Environ. 142, 43–56. https://doi.org/10.1016/j.atmosenv.2016.07.040

Wu, Z., Zhang, S. (2019). Study on the spatial–temporal change characteristics and influence factors of fog and haze pollution based on GAM. Neural Comput. Appl. 31, 1619–1631. https://doi.org/10.1007/s00521-018-3532-z

Xiang, P., Zhou, X., Duan, J., Tan, J., He, K., Yuan, C., Ma, Y., Zhang, Y. (2017). Chemical characteristics of water-soluble organic compounds (WSOC) in $PM_{2.5}$ in Beijing, China: 2011–2012. Atmos. Res. 183, 104–112. https://doi.org/10.1016/j.atmosres.2016.08.020

Xu, P.J., Wang, W.X., Yang, L.X., Zhang, Q.Z., Gao, R., Wang, X.F., Nie, W., Gao, X.M. (2011). Aerosol size distributions in urban Jinan: Seasonal characteristics and variations between weekdays and weekends in a heavily polluted atmosphere. Environ. Monit. Assess. 179, 443–456. https://doi.org/10.1007/s10661-010-1747-2

Yang, D.Y., Liu, B.X., Zhang, D.W., Chen, Y.Y., Zhou, J.N., Liang, Y.P. (2015). Correlation, seasonal and temporal variation of water-soluble ions of $PM_{2.5}$ in Beijing during 2012-2013. Huan Jing Ke Xue 36, 768–773. (in Chinese)

Yu, M.Y., Xu, Y., Li, J.Q., Lu, X.C., Xing, H.Q., Ma, M.L. (2021). Geographic detector-based spatiotemporal variation and influence factors analysis of $PM_{2.5}$ in Shandong, China. Pol. J. Environ. Stud. 30, 463–475. https://doi.org/10.15244/pjoes/120522

Zalakeviciute, R., López-Villada, J., Rybarczyk, Y. (2018). Contrasted effects of relative humidity and precipitation on urban $PM_{2.5}$ pollution in high elevation urban areas. Sustainability 10, 2064. https://doi.org/10.3390/su10062064

Zhai, S., Jacob, D.J., Wang, X., Shen, L., Li, K., Zhang, Y., Gui, K., Zhao, T., Liao, H. (2019). Fine particle matter ($PM_{2.5}$) trends in China, 2013–2018: separating contributions from anthropogenic emissions and meteorology. Atmos. Chem. Phys. 19, 11031–11041. https://doi.org/10.5194/acp-19-11031-2019

Zhang, H., Wang, Y., Hu, J., Ying, Q., Hu, X.M. (2015a). Relationships between meteorological parameters and criteria air pollutants in three megacities in China. Environ. Res. 140, 242–254. https://doi.org/10.1016/j.envres.2015.04.004

Zhang, Q., Streets, D.G., He, K., Klimont, Z. (2007). Major components of China's anthropogenic primary particulate emissions. Environ. Res. Lett. 2, 045027. https://doi.org/10.1088/1748-9326/2/4/045027

Zhang, R., Wang, G., Guo, S., Zamora, M.L., Ying, Q., Lin, Y., Wang, W., Hu, M., Wang, Y. (2015b). Formation of urban fine particle matter. Chem. Rev. 115, 3803–3855. https://doi.org/10.1021/acs.chemrev.5b00067